Sea-Salt Size Distributions from Breaking Waves: Implications for Marine Aerosol Production and Optical Extinction Measurements during SEAS*

A. CLARKE, V. KAPUSTIN, S. HOWELL, AND K. MOORE

Department of Oceanography, University of Hawaii at Manoa, Honolulu, Hawaii

B. LIENERT

Hawaii Institute of Geophysics and Planetology, University of Hawaii at Manoa, Honolulu, Hawaii

S. MASONIS, T. ANDERSON, AND D. COVERT

Department of Atmospheric Sciences, University of Washington, Seattle, Washington

(Manuscript received 16 July 2002, in final form 14 February 2003)

ABSTRACT

The authors' participation in the Shoreline Environment Aerosol Study (SEAS) involved measurements focused on the coastal aerosol size distribution and related optical measurements, including aerosol light scattering, visibility, and remote sensing of aerosol using lidar backscatter. Aerosol production from shoreline breaking waves and the more distant reef (~1 km) was characterized for dry sizes between 0.01 and 10 μm for both their contribution to the marine aerosol population and their influence on near-surface lidar extinction. Thermal volatility was used to extract the refractory sea-salt particles from the other constituents volatile at 360°C. At 7 m ASL and 20 m inland from the water's edge the production of sea-salt nuclei number was often in the range of 50–100 cm^{-3} above the open-ocean value of ~250 cm^{-3}. This number peak was near 0.03-μm dry diameter, while light scattering was dominated by a few particles larger than 1 μm. This indicates that production of sea salt from breaking waves contributes not only to aerosol mass and optical effects but also to nuclei mode particle number in remote regions. Separate studies of optical closure quantified links between the size distribution and optical scattering measurements, visibility, and extinction values for both nearshore breaking waves and open-ocean conditions. These data confirmed that extinction derived from coastal lidar measurements at 0.530 μm was accurate to better than the 25% uncertainty claimed for the lidar inversion.

1. Introduction

The Shoreline Environment Aerosol Study (SEAS) took place at Bellows Air Force Station (BAFS) on the east coast of Oahu, Hawaii, 21–30 April 2000. The site description, sampling considerations, and environmental factors influencing coastal aerosol production, as well as the involvement of other SEAS participants, are discussed elsewhere (Clarke and Kapustin 2003). Here we focus on marine aerosol size distributions and their link to optical properties. A variety of instruments were used to measure aerosol over the size range from 0.01 μm to over 10 μm, a range of about 10 orders of magnitude in aerosol mass. We will first address the smallest size range below about 0.1 μm that was found to dominate sea-salt number and then the larger range of 0.1–10 μm or so that dominates near-surface marine aerosol mass and its optical properties.

The University of Hawaii (UH) sampling was carried out from the 20-m BAFS tower (Fig. 1a) through a 5-cm-diameter polyvinyl chloride (PVC) sample line. This transported aerosol to our research van that housed our instruments at the base of the tower (Clarke and Kapustin 2003). Three solenoid-activated diaphragm valves with large apertures of about 4 cm^2 were mounted on the tower to provide selective sampling from 5-, 10-, and 20-m (7, 12, and 22 m ASL) elevations. Each valve controlled flow in a 2.5-cm-diameter PVC inlet tube oriented at a 45° downward angle. The inlet opening was parallel to the northeast trade wind that blew nearly orthogonal to the coast at this location (Clarke and Kapustin 2003). Inlets were attached to a 5-cm PVC sampling tube running down the length of the tower. Each valve was sampled sequentially for 20 min out of each hour in order

* School of Ocean and Earth Science and Technology Contribution Number 6066.

Corresponding author address: Dr. A. Clarke, Department of Oceanography, University of Hawaii at Manoa, 1000 Pope Rd., MSB 501, Honolulu, HI 96822.
E-mail: tclarke@soest.hawaii.edu

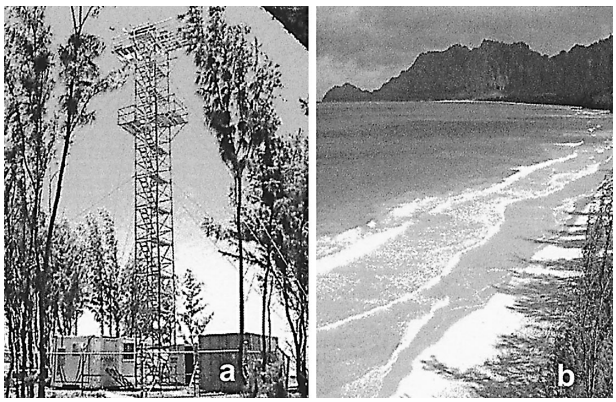

FIG. 1. (a) View from the landward side of the BAFS 20-m sampling tower with UH inlets at 5, 10, and 20 m and (b) a view of the coastal breaking waves taken from the top of the tower.

to obtain both temporal and vertical variations in the aerosol field. Air sampled through the bottom valve was generally influenced by nearby shoreline breaking waves (Fig. 1b), while the higher valves were not, even though all were often influenced by other sources such as the upwind reef areas (Clarke and Kapustin 2003).

The UH sample line terminated inside the portable laboratory van at the base of the tower. Several smaller tubes were mounted near the center of the PVC sample line flow, with diameters designed to allow for near-isokinetic sampling to various instruments. The largest flow of 30 L min^{-1} went to a three-wavelength integrating nephelometer (Model 3563, TSI, Inc.). An impactor with aerodynamic size cut at 1 μm was alternately inserted into this flow path to periodically remove the larger aerosol in order to resolve contributions to scattering from particles above and below this size. This nephelometer generally operated near 55% relative humidity (RH) compared to ambient values that were usually in the 70%–85% range. Another enclosed nephelometer [University of Washington (UW)] near 10 m on the tower operated closer to ambient RH (Masonis et al. 2003). Two condensation nuclei (CN) counters recorded particle number concentrations at 50°C (CNcold) and 360°C (CNhot). This allowed refractory particles remaining after heating to 360°C, such as sea salt, to be distinguished from more volatile species such as sulfates with a 1-Hz time resolution. Other supportive measurements such as wind speed, wind direction, relative humidity, precipitation, tides, pressure, sunlight, and meteorological parameters were also recorded.

Size distributions were determined with an aerodynamic particle sizer (APS; Model 3320, TSI, Inc.; $0.5 < D_p < 10$ μm), a radial differential mobility analyzer (RDMA; $0.007 < D_p < 0.3$ μm) (Zhang et al. 1995) and a laser optical particle counter (OPC; $0.1 < D_p < 7$ μm). The RDMA places a Boltzmann charge distribution on the aerosol and then sizes the particles on the basis of their mobility in an electric field. Both the OPC and RDMA employed thermal volatility to measure distributions in air sampled at about 50°, 150°, and 360°C. This established the volatile particle fractions (Clarke 1991) and left the refractory sea-salt distribution at 360°C. The UH lidar periodically operated over a range of angles, distances, and altitudes during SEAS and detected aerosol produced from breaking waves (if focused just downwind of the reef or along the coast) as well as open-ocean conditions (Porter et al. 2003). Because a major SEAS objective was to link the in situ data to lidar observations, many lidar measurements were made at about a 58° azimuth in a vertical scanning mode to explore vertical development of aerosol plumes downwind of the reef and moving toward the tower. Even so, the variable wind directions, wind speeds, and aerosol plume structures (Clarke and Kapustin 2003; Porter et al. 2003) meant that the lidar and the wind direction bringing aerosol to the tower were only rarely in alignment. A direct comparison of these measurements is also problematic since plumes evolve, mix, and dilute during transport to the tower from the location at which the lidar probed them. Here we describe a long-term statistical assessment accomplished by sampling from the three tower locations as a means to evaluate in situ and lidar extinction data. This provided data ranging from conditions similar to breaking waves collected near the bottom of the tower to open-ocean conditions approximated by sampling at the top (20 m). Of course, when waves were breaking on the offshore reef about 1.5 km away, even the 20-m data could be influenced by evolving plumes from the reef.

During SEAS the UH instruments collected data by cycling through the three tower altitudes using uniform inlets, while other SEAS investigators sampled from the tower at single (albeit various) altitudes with diverse individual inlets. Hence, the UH measurements could observe production of nearshore aerosol from isolated breaking waves at the base of the tower after removing the open-ocean contribution derived from the top of the tower. This approach allowed direct assessment of the impact of shoreline breaking waves on aerosol production as a function of size. These coastal waves were generally small during the SEAS period (~0.5 m) and were breaking about 20–25 m from the shore to produce foam for about 20–30 s before dissipating on the shore (Fig. 1b). Wave fronts were variable and often separated by about 10 m, but overlapping waves were common. These wave heights were often less than wave heights in the reef region, but the 20 m of foam exposure is similar to that on the reef about 1.5 km away [see Fig. 1 of Clarke and Kapustin (2003)]. This similarity allows us to use breaking-wave data from the lowest tower inlet as a surrogate for contributions from similar waves produced in the reef region.

2. Sampling issues

Quantitative comparisons of independently measured and remotely sensed properties require proper calibra-

tions, corrections, and transformations to appropriate measurement conditions. The change in marine aerosol size with RH is one issue that affects many physical, chemical, and optical properties of the marine aerosol examined during SEAS. Water uptake influences aerosol size, density, and refractive index in various ways. This impacts the interpretation of data from various instruments and the extrapolation of measured data to ambient conditions (Clarke et al. 2002). Some sizing instruments were nominally ''dry'' in the sense that they measured at low RH (but often different) with relatively little water volume associated with them. Other instruments (e.g., nephelometers) were at intermediate humidity, while the lidar was at ambient conditions near 80% RH. The following discussions will include procedures used to establish appropriate size distributions and scattering extinction values for comparison to other instruments during SEAS.

The RDMA, OPC, and APS size distributions were measured at instrument RH. The RDMA employed a dessicated sheath air sample flow to bring RH to about 25% for sizing. The OPC mixed sample and dessicated air upstream of the instrument in order to lower RH to about 30%–50% so that particulate water was minimized. The APS internal heating to 30°–32°C resulted in RH near 50% but generally above the efflorescence point of sea salt (Tang et al. 1997). The original calibration for all instruments employed latex calibration spheres with a refractive index of 1.588 and density of 1.05 g cm^{-3}. After adjustments to reference ''dry'' (RH = 40%) diameters we combined data from these instruments to provide sizing over the ranges 0.007–0.15, 0.15–0.75, and 0.75–12.0 μm, respectively. A number of steps are required in order to utilize the combined measured size distributions for modeling aerosol optical properties. As detailed below, these generally include one or more corrections for 1) measured versus calibration aerosol properties, 2) measured versus desired humidity conditions, 3) size-dependent instrument performance, and 4) size-dependent sampling issues.

a. RDMA sizing

The RDMA sizes charged particles between 0.007 and 0.250 μm based upon the mobility of aerosol in an electric field (Zhang et al. 1995). We limit consideration of these data to the 0.010–0.15-μm range, where concerns over diffusive losses (smaller sizes) and charging efficiency (larger sizes) are of secondary importance to the data presented here. RDMA diameters were corrected from instrument RH to RH = 40% using the growth factor, $g(\mathrm{RH}) = (1 - \mathrm{RH})^{-0.210}$, measured by Swietlicki et al. (2000) for marine aerosol. The RDMA was used in conjunction with a lagged aerosol grab (LAG) chamber (Clarke et al. 1998) that ''captured'' a sample of air over about 15 s for subsequent thermal analysis over several minutes. This allowed the rapid collection of aerosol from individual breaking waves and ensured that temporal variation in the sample did not occur during the 3-min measurement period needed for thermal RDMA analysis, a critical requirement to sample plumes from breaking waves having only a 15–60-s duration.

b. OPC sizing

The OPC (LAS-X, Particle Measurement System, Inc., with custom electronics) sizes are based upon scattering from dry latex calibration spheres with a refractive index of 1.588 at 0.632 μm. These were corrected to account for the refractive index under measurement conditions assuming a nonabsorbing sulfate aerosol at particle sizes below 0.6 μm and a sea-salt aerosol above. A linear transition in composition was assumed between 0.45 and 0.7 μm as suggested by our volatility data (see section 3b). The refractive index below 0.45 μm is modeled using partial molar refractions (Stelson 1990), assuming a sulfate aerosol mix expected for a clean marine environment (''SH marine temperate''; Quinn et al. 2001). Above 0.7 μm we assume a sea-salt aerosol with humidity growth dependencies established by Tang et al. (1997).

OPC diameters were corrected to account for the appropriate refractive index, m. This was adjusted from the calibration value of 1.588 to the refractive index at the OPC measurement RH using a scaling coefficient f_D, given as ($f_D = 1.76\ m^2 - 5.99\ m + 6.04$) (Hand et al. 2000). After refractive index correction the OPC diameters were shifted to 40% RH using accumulation-mode (Swietlicki et al. 2000) and sea-salt (Tang et al. 1977) growth factors. Although our OPC data have been generally found to be representative of ambient aerosol up to about 5-μm diameter in previous studies, we believe that the tubing and heating system used during SEAS compromised transmission to the OPC for sizes above about 0.75 μm. Hence, we only report OPC data up to 0.75 μm, and data for larger sizes are obtained from the APS during SEAS.

c. APS sizing

APS diameters were converted from aerodynamic diameter to geometric diameter assuming a density for wetted sea salt at measured APS RH (Tang et al. 1997). The combined RDMA, OPC, and APS distributions yielded a composite distribution at 40% RH with a uniform log$D$ scale of 50 diameter steps per decade and 167 diameters altogether. Growth from 40% RH to ambient RH was then applied to combined size distributions using Swietlicki's g(RH) for accumulation mode and sea-salt g(RH) for sea-salt mode (accumulation/sea-salt modes cut at 0.6 μm). It is important to note that the APS used during SEAS (and by many other investigators) was TSI Model 3320, now recognized to exhibit ''ghost'' particle counts in larger sizes (M. Havlicek, TSI, 2000, personal communication). New tech-

nology in the replacement model TSI 3320a tested at BAFS after SEAS did not have this problem, so these results were used to correct our original coarse particle size distributions, as discussed in section 3c.

d. Inlet losses

Aerosol sampling systems often lose particles over certain size ranges as a result of diffusion, inlet configuration, anisokinetic sampling, sedimentation, impaction, etc. These latter effects are often greatest for large particles. Because breaking waves often generate large particles that can affect aerosol optics (Reid et al. 2001; de Leeuw et al. 2000; Vignati et al. 2001), we expect losses for larger sizes in our tower system. We first compare losses for the UW and the UH inlet systems using the APS at the common height of 10 m. Next, we will discuss post-SEAS data from the APS exposed directly to ambient aerosol and using only a small isokinetic sample inlet. The results will be used to correct and interpret coarse-particle data obtained from our sampling system.

e. Nephelometer

The UH and UW TSI 3563 integrating nephelometers measure light scattering at three wavelengths (450, 550, 700 nm) over an angular range of about 7°–173°. Because coarse sea-salt particles have a scattering phase function that includes significant forward scatter at less than 7° (Porter et al. 2003), the instrument must be corrected for this angular truncation error, as discussed elsewhere (Anderson and Ogren 1998; Masonis et al. 2003), before comparing to integral scattering values derived from size distributions. In order to measure both coarse- and fine-particle scattering an impactor was used here ahead of the nephelometer to remove large particles above a 1-μm aerodynamic cut size. The corresponding physical ''dry'' size as detected by the OPC depends upon humidity but represents a geometric size of about 0.75 μm during much of SEAS. Because this size cut is not sharp and occurs at a diameter at which coarse sea-salt mass can increase rapidly, we have applied a sigmoid cut more representative of a Berner-type impactor (Berner et al. 1979) in our analysis.

3. Observations

a. Representative tower data and aerosol microphysics

Measurements from the various tower altitudes reveal clear differences in number concentrations, particle volumes, and associated optical properties (Fig. 2). At the lowest altitude (valve t1), excursions in CN of about 50 cm^{-3} are associated with production from breaking waves. Heated CN shows similar excursions, while the difference between heated and unheated CN is nearly

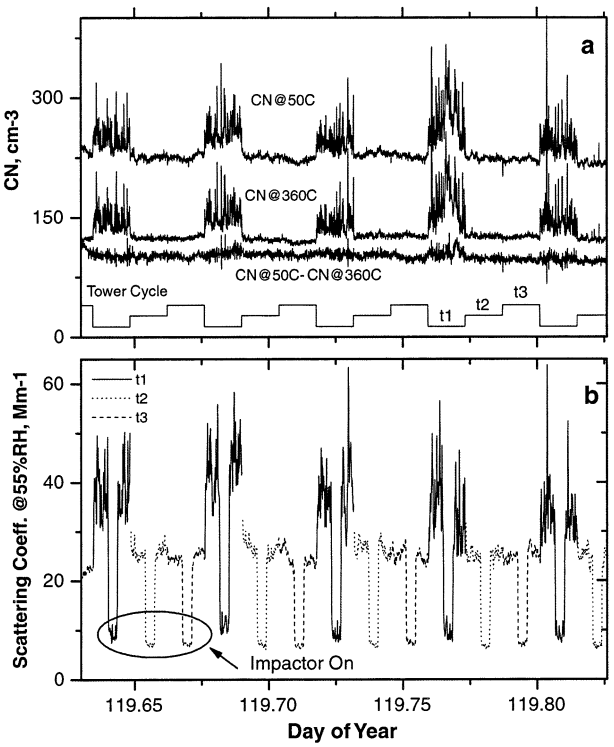

FIG. 2. A time series indicating multiple cycles through the three tower sample valves (t1, t2, t3) over a 5-h period for (top) measured CN at 50° and 360°C and their difference and (bottom) for concurrent light scattering.

constant and similar to values at heights unperturbed by these breaking waves. Hence, most CN produced by breaking waves are refractory, as expected for a sea-salt aerosol at 360°C, and are superimposed upon a more volatile and less variable background aerosol that constitutes about 40% of the total CN.

Aerosol light scattering (corrected for truncation errors) for the same period (Fig. 2b) is interrupted by a 5-min period when the impactor (1-μm aerodynamic cut size) is inserted into the flow. This removes the coarse particles to reveal the submicrometer scattering data. These data also show that shoreline waves enhance total scattering at 5 m by up to a factor of 2 compared to other levels. Data obtained after the impactor for the lowest valve t1 show similar short-period fluctuations from waves and an enhancement of 30% ± 10% compared to other levels, an indication of the optical influence of submicrometer sea-salt aerosol at 0.55 μm. The 10- and 20-m tower data are similar but with occasional but consistent enhancements of 10% or so for the 10-m inlet position, indicating weak but occasional breaking-wave influence at this altitude.

An expanded 1-h time series sampled every 5 s (Figs. 3a,b) better reveals concurrent variations in both CN and nephelometer light scattering (~55% RH) at all three tower altitudes, including 5-min impactor data. However, the nephelometer internal volume (~3 L), the

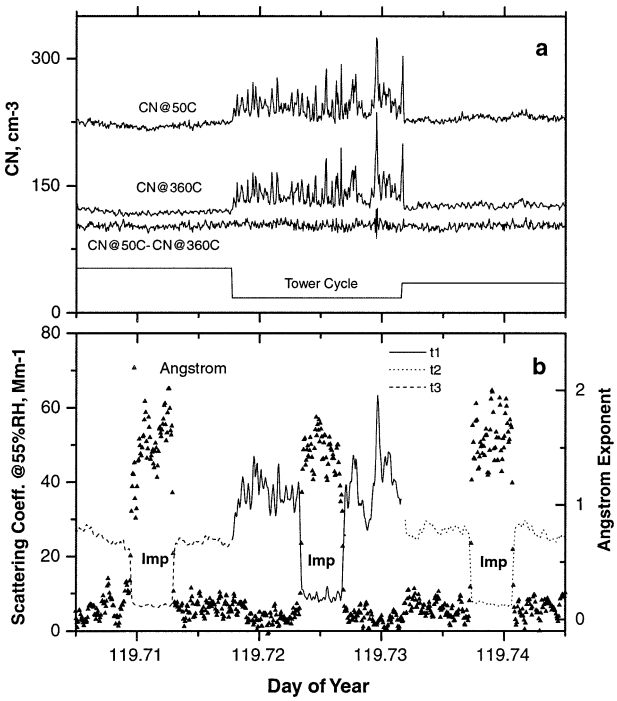

FIG. 3. A 1-h time series showing (a) CN at 50° and 360°C and their difference and (b) scattering extinction with 5-min impactor period (Imp) and the Ångström exponent for each 20-min valve cycle.

30 L min^{-1} flow rate, and the temporal averaging of 10 s result in an effective delay of about 15 s and a smoothing (broadening) of scattering compared to CN data. The 5-s CN data at 5 m better resolves aerosol plume structures as short as 15 s. Some periods reveal overlapping peaks lasting up to about a minute, consistent with variable production from multiple waves breaking along the shore (Fig. 1b).

Concurrent excursions in CNhot and CNcold for breaking waves at 5 m (Fig. 3a) show similar magnitudes for each breaking-wave event. The difference between CNcold and CNhot (more volatile aerosol component) is nearly constant and reflects a different origin for these background volatile nuclei present at all tower altitudes. These features demonstrate that wave-produced particles are all refractory, as expected for sea salt at 360°C. Excursions in these salt nuclei concentrations at 5 m typically range from about 20 to over 100 cm^{-3} for these small coastal waves. Concurrent variations are evident in CN and light scattering data (slightly delayed and broadened because of residence time in the nephelometer) for both total and submicrometer aerosol at 5 m. These waves break, produce foam, and dissipate over about 20 m (Fig. 1b) and enhance the 5-m CN concentrations at the tower by about 25%–50% and light scattering by about 50%–100% over open-ocean values. However, as shown below, the light scattering is usually dominated by just a few particles present in the large particle size range.

The wavelength dependence of light scattering measured by the UH TSI nephelometer can be described by the Ångström exponent. This is given as the negative difference in logarithm of scattering divided by the difference in the logarithm of the wavelengths (see Masonis et al. 2003). The values tend to near zero for large aerosols and to values near 2 when only small aerosols are significant. The Ångström exponent for this 1-h period is shown in Fig. 3b where the impactor demonstrates this variation when large aerosols are removed. The domination of total scattering by coarse aerosol (Fig. 2b) is also revealed here by the Ångström exponents near zero for all tower altitudes. Lowest values are most evident for the 5-m altitude data where short-period increases in scatter from breaking wave events can drive the Ångström exponent to its lowest values [e.g., see data near day of year (DOY) 119.73].

b. Size distributions produced from breaking waves

As described earlier, the full-size distributions were obtained from a combination of instruments including the RDMA and OPC equipped with thermal analysis to help resolve refractory constituents and to infer composition (Clarke 1991). These are shown here as measured at so-called dry RH. In order to isolate size distributions produced from the nearshore breaking waves we examined differences between average size distributions accumulated at both the top and bottom of the tower. Here we show (Fig. 4) examples for the 5-h period on DOY 119 shown in Fig. 2. In this linear format of $dN/d\log D_p$ versus $\log D_p$ the areas under the curves are proportional to total number and best reveal the small-particle contribution, while the logarithmic format provides concentration information over a greater range of particle sizes. To best evaluate production at the smallest particle sizes, we picked a period in which repeated opening of the LAG chamber (about 15 s each) for the RDMA coincided with numerous breaking-wave peaks at 5 m so that the resulting averaged small-particle size distribution was stable, well resolved, and most representative of these breaking waves. These combined RDMA and OPC thermally resolved data include approximately 15–20 LAG chamber samples (depending on time coordination) from the 5- and 20-m tower altitudes during this period. The unheated distributions appear to be bimodal, with a smaller peak near 40-nm diameter and a larger one near 150 nm.

The heated distributions at both tower altitudes are shifted to smaller sizes for particles below about 0.5 μm, while larger sizes are relatively unaffected. These large sizes are refractory sea salt, while smaller sizes are often mixtures of sea salt with volatile species (e.g., sulfates) and other components. Note that about 60% of the number remains after heating at both altitudes, consistent with the observed disappearance of 40% of the measured CN upon heating (Figs. 2 and 3). Since DOY 119 is during the period of long-range transport of volcanic emissions from over Japan (Clarke and Kapustin

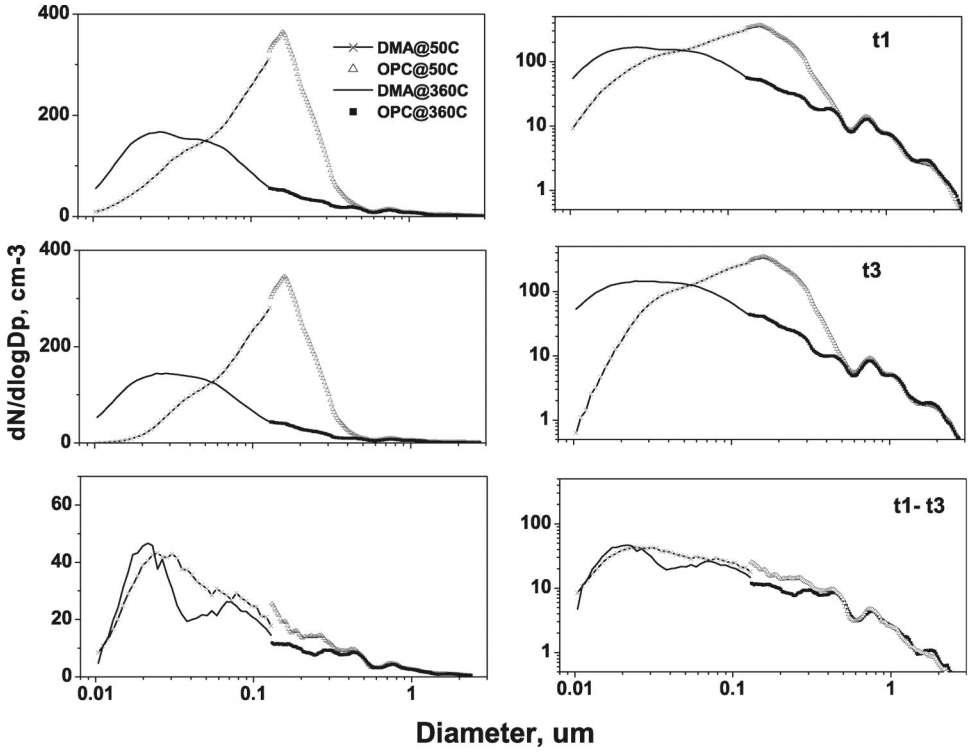

FIG. 4. Dry number size distributions (DOY 119) measured at (top) 5 and (middle) 20 m and (bottom) their difference for unheated (50°C) and heated refractory distributions (360°C) in both linear and logarithmic concentration formats (10-point-diameter smoothing applied).

2003), refractory species other than sea salt are possible. Such thermally resolved sea-salt sizes (Clarke et al. 1993; O'Dowd et al. 1997) also provide a tool for interpreting other measurements of sea salt (Campuzano-Jost et al. 2003).

The contribution of coastal breaking waves is clearly revealed by the difference between number distributions at 20 and 5 m (Fig. 4, lower panels). The unheated difference distribution demonstrates that breaking waves produce particles from as small as 0.01 μm (dry diameter) up to several micrometers (larger sizes not shown here) and with a number peak near 0.03–0.40 μm. The heated difference distributions show that most of these are refractory at 360°C, consistent with their being sea salt. The average heated and unheated difference distributions are similar in both their number and shape, indicating that these small particles produced are refractory. The lower number at the smallest sizes for the RDMA measurements is presumably due to the 360°C RDMA scan always being the last sample from the LAG chamber, leading to diffusive losses for smaller particles that have not been corrected for here. Even so, the integral number of about 30–40 cm^{-3} is consistent with the typical number peaks evident in the CNcold and CNhot from breaking waves at the 5-m level (Fig. 3). The shapes of these difference distributions are also similar to the total refractory distributions measured at both altitudes. This suggests that sea salt from breaking waves in open-ocean conditions probably contributes to these refractory aerosols. These sizes are far smaller than the 0.1–0.2-μm diameters often referenced in the literature for the smallest sizes of sea-salt size distributions (Hoppel et al. 2002, and references therein).

Coarse particles from breaking waves were also characterized through similar differencing of data collected at the top and bottom of the tower. However, because concentrations are much lower for coarse aerosol, we use averages of each 20-min sample from each altitude accumulated over many hourly cycles. These coarse-particle distributions also require some corrections for inlet losses of coarse particles, as discussed below. Resulting difference distributions for the bottom less the top of the tower are shown in Fig. 5a as number distributions on a logarithmic scale. The sea-salt mass and the sizes that dominate observed scattering are best revealed in Fig. 5b as linear volume distributions (multiply the scale by about 2 to estimate area under curve as dry mass in $\mu g\ m^{-3}$). These difference distributions show that these coastal breaking waves produce aerosol dry mass that peaked near 7 μm. If growth to typical ambient humidity (RH 80%) is estimated for the dry sizes shown here, they would nearly double in size. The resulting concentration and the falloff in coarse-particle number concentration with size would be very similar to the recently published ambient data of Hoppel et al. (2002) for 10 m s^{-1} near-surface winds.

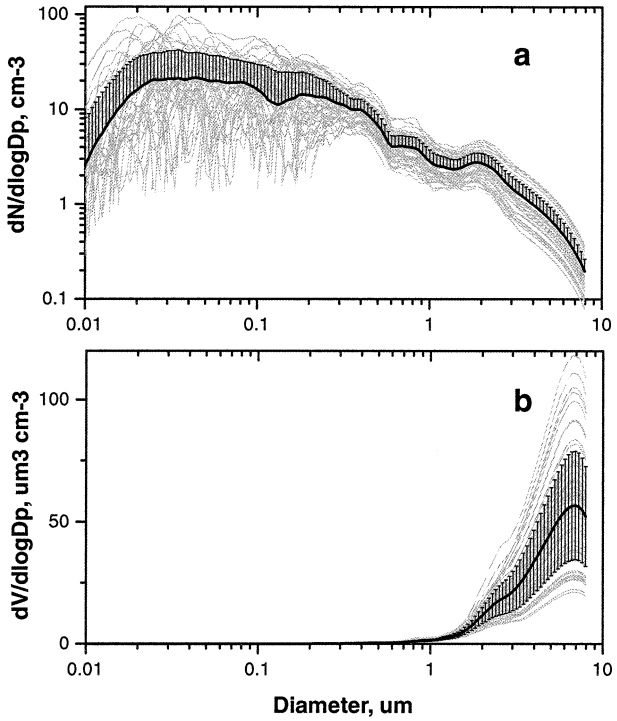

FIG. 5. A superposition of dry (a) number and (b) volume size distributions obtained by differencing the average 5- and 20-m tower data obtained for each hourly cycle during SEAS. The transmission correction to the UH inlet has been applied. Single leg std dev shown on log plot for clarity.

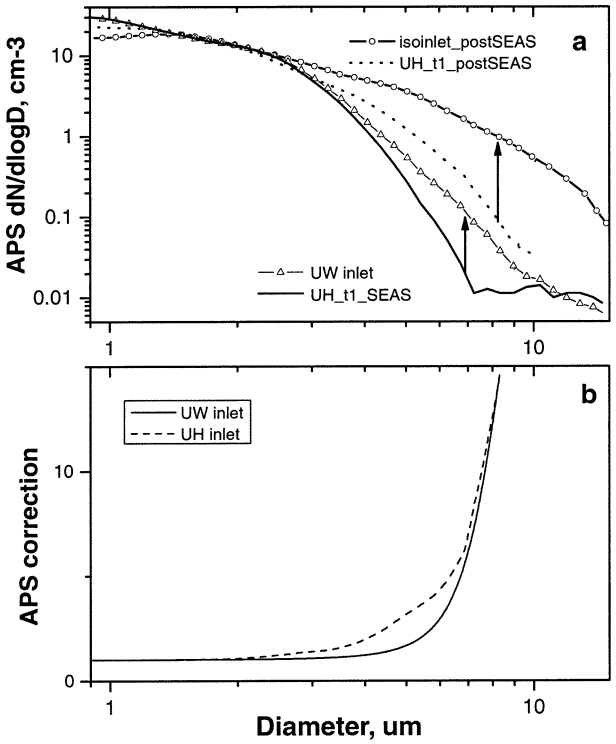

FIG. 6. (a) Comparison of measured APS size data for UH tower inlet t1 (solid line) vs UW inlet (triangles) during SEAS using an old APS with a ''ghost'' particle counting problem, and a similar post-SEAS comparison for a new APS (no inlet) vs UH tower inlet t1 measured with new APS. Arrows indicate curves to be compared in each case (see text). (b) APS inlet correction factor based upon data in (a).

c. Inlets, size distributions, and calibration issues

The UH and UW inlets were different, and an assessment of inlet performance as a function of aerosol size is needed if quantitative comparison to ambient conditions is attempted for the UW nephelometer. The inlet to the UW nephelometer did not have the valves present in the UH system. Also the UH system employed a PVC tube located at about 10 m on the tower compared to about 11 m for the UW nephelometer (Masonis et al. 2003) that also operated at a higher RH. In order to test for sampling differences in the UH and UW inlets under similar conditions the APS was removed from the UH inlet and operated on the UW inlet upstream of the UW nephelometer and then returned to the UH inlet. Comparison of APS size data (Fig. 6a) at 55% RH for the UH and UW inlets during SEAS shows that both inlets had similar transmission (Fig. 6b) for particles sizes up to about 2 μm. Above that size, the UH system was less efficient up to about 7 μm. Figure 6b shows the different size-dependent corrections used for UH and UW inlets based upon the ratio between the UH (t3) and UW inlets. Above 7 μm, the UH inlet sizes show a sudden inflection and evidence of irregular counting that is nearly constant with size. Similar behavior is also evident above 10 μm for the same APS on the UW inlet. We now believe that this behavior is linked to ''ghost'' particles circulating inside the APS sensing volume that yield pulses interpreted as additional larger aerosol at random sizes (M. Havlicek, TSI, 2000, personal communication). These are most conspicuous when the actual large-particle concentrations are low, and they result in a combination of real and artifact counts at larger sizes that are difficult to separate.

The new TSI APS Model 3321 corrects this ''ghost'' problem and was deployed after SEAS on 2 April 2002, under similar conditions at the BAFS tower and operated with a short 10-cm isokinetic inlet directly into the wind (about 3 m s^{-1}) at 5 m (tl). Figure 6a shows size distributions collected over 30 min from this inlet (isoinlet_post SEAS) and those after sequential sampling for 30 min through the SEAS 5-m inlet (UH_t1_post SEAS). These distributions are normalized to sizes at 1.5 μm, where inlet losses are not evident, in order to compare to data from different periods. This comparison confirms both the unrealistic shape of the distributions for the SEAS data above about 7 μm as well as the significant coarse-particle losses through the SEAS inlet. Hence the SEAS tower size data suffered from loss of coarse particles in the inlet that reduced coarse concentrations to where ghost particles artificially enhanced coarse concentrations over those present at the APS. Figure 6a reveals that a direct correction of APS data above 7 μm

is hard to justify. At the same time it is clear that particles are certainly present at these larger sizes.

Correcting for this is important to the objective of comparing tower and lidar data since optical properties will be strongly influenced by particles in this size range. The correction is constrained by the post-SEAS measurements just described. Our approach builds upon the observations previously discussed for breaking-wave events, where we demonstrated that these events generate particles across the entire size spectrum. This is also evident in the concurrent increases in CN (dominated by small particles) and scattering (dominated by large particles) in Figs. 2 and 3 and observed consistently throughout the experiment. We argue that increases observed in the APS sea-salt concentrations near 3 μm reflect similar increases across the spectrum and that in this size range any possible variations in other species present in the accumulation mode (e.g., sulfate) will not be contributing. Furthermore, the constancy of the standard deviation in APS concentrations over the 0.7–3.0-μm-diameter range (Fig. 5a) is consistent with variations in concentrations occurring simultaneously across the entire coarse size range. This is evident when variations in sequential distributions are examined (not shown). Hence, we have taken our 20-min average APS values at 3 μm (''dry'' size) during each 1-h valve cycle and scaled the 30-min average post-SEAS distribution in Fig. 6a to merge with it. This allows us to extend our distributions to the 8-μm dry sizes shown in Fig. 5. This assumes that the shape of the size distribution is invariant for the limited range of conditions encountered during SEAS and that relative increases seen at 3 μm in the dry sizes extend to 7 μm.

d. Aerosol optics and size distributions

The aforementioned observations were for aerosol sizes as measured without correction for RH. Because RH has such a significant effect on marine aerosol size we generally operate instruments such as the RDMA and OPC in the dry mode at less than 40% RH so that sizes and refractive indices are close to dry mass properties. Then, as described earlier, appropriate ancillary information is used to ''grow'' particles to larger sizes at a given RH. Before comparing measured size distributions to other measurements (e.g., SEAS lidar) it is important to evaluate size data by testing it against concurrently measured optical data (e.g., nephelometer light scattering). This constitutes a ''local closure'' by using the combined size distribution, size resolved chemistry, and associated refractive indices to model aerosol light scattering at the nephelometer RH using the same tower inlet system. If the resulting calculated scattering and the wavelength dependence expressed by the Ångström exponent agree with values measured by the nephelometer, then our physiochemical description of the aerosol is appropriate for the related optical properties.

The total measured size distribution at nephelometer RH has been used to model expected scattering extinction for RH in the UH and UW nephelometers, including correction for the different transmission efficiency of the UW inlet system. Particle diameter growth resulting from changes in RH must be considered. Examples of the impact of RH on scattering or so-called f(RH) are based upon measurements hygroscopic growth (Swietliki et al. 2000) for the clean marine submicrometer mode and for sea salt (Tang et al. 1997).

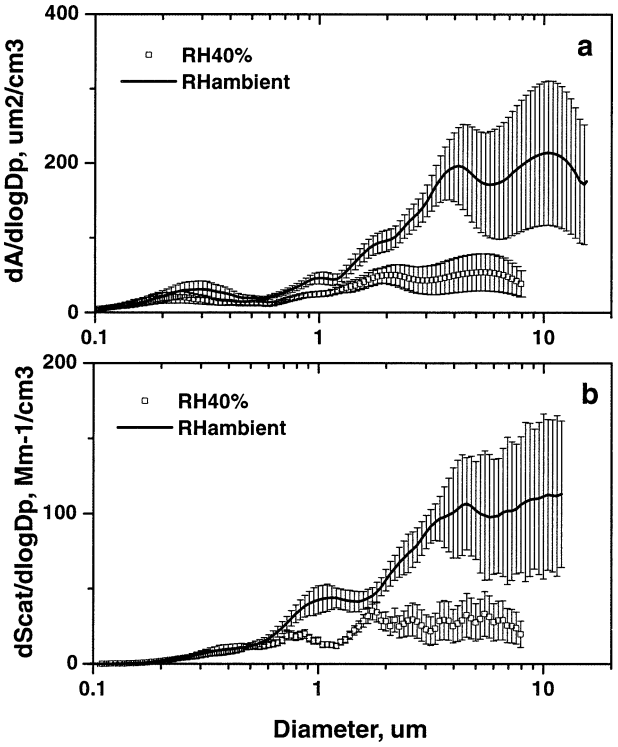

FIG. 7. Comparison of (a) surface area and (b) calculated scattering distributions over size for both dry 40% RH and ambient humidity conditions during the first half of the SEAS experiment.

Figure 7 shows the average size distribution and standard deviation at 5 m for the ''clean marine period'' DOYs 110–117 (see Clarke and Kapustin 2003). These are shown as surface area (Fig. 7a) at 40% RH and at ambient RH after correcting for ambient RH conditions during each case before averaging. These distributions are used for Mie scattering calculations to yield the corresponding scattering distributions (Fig. 7b) (dScat/$d\log D_p$ versus $\log D_p$) for ''dry'' and ''ambient wet'' conditions such that the area under each plot is proportional to scattering extinction. The more irregular structure in the scattering plots with size is a result of the Mie scattering variations that will also occur in the atmosphere.

e. Size and nephelometer closure

Our light absorption values were low during SEAS with slightly higher values after DOY 118 when influ-

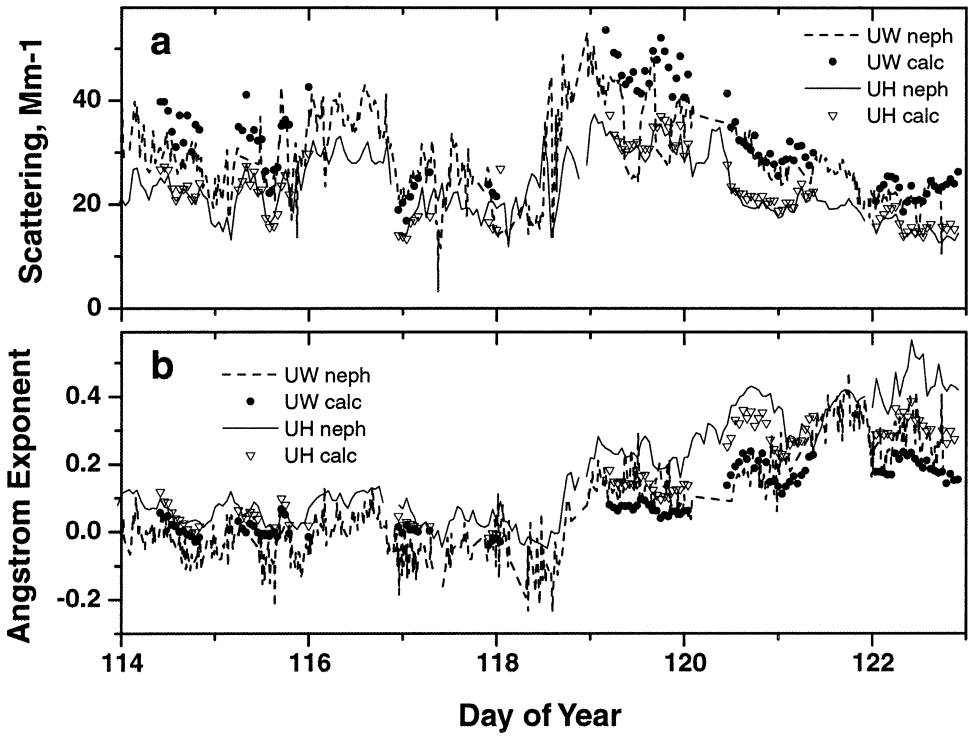

FIG. 8. Time series for (a) measured scattering and (b) the Ångström exponent determined from the UW and UH nephelometers and from corresponding size distributions corrected to nephelometer RH.

enced by long-range transport (Clarke and Kapustin 2003). These are consistent with those reported elsewhere (Masonis et al. 2003) and will not be repeated here. Hence, scattering extinction was nearly equal to the total extinction during SEAS, prompting us to use these terms interchangeably hereafter. The UH and UW nephelometer datasets corrected for angular truncation error (Anderson and Ogren 1998) are shown in Fig. 8a, and the difference is due primarily to their operation at different RH values and also to the different inlet losses discussed previously. Scattering values calculated from size distributions at each nephelometer RH are shown for measured UH and UW scattering and reveal good agreement. Similar good agreement is shown for the Ångström coefficient (Fig. 8b) but with values derived from the size distribution becoming somewhat less than the nephelometer after DOY 118. Note that both measured and model values increase after DOY 119, reflecting changes in the aerosol size distribution as a result of long-range transport of volcanic aerosol from Japan (Clarke and Kapustin 2003). This ''closure assessment'' indicates that the size distributions, their composition, growth, and calculated optical properties are quite consistent with measured optical properties.

4. Comparison of in situ data with lidar extinction

a. Time series comparisons

This aforementioned ''closure'' provides a basis for modeling aerosol optics at ambient conditions, as needed for comparison to lidar data, a SEAS objective. Separate papers discuss the details of the lidar retrievals (Porter et al. 2003) and independent evaluations of the lidar backscatter coefficient (Masonis et al. 2003). Direct comparisons of in situ tower data and lidar measurements during SEAS are complicated by the fact that the lidar data are obtained from a region 300–400 m or more offshore. A quantitative comparison is therefore questionable because of the roles of mixing, dispersion, dilution, and meandering winds (see Clarke and Kapustin 2003; Porter et al. 2003).

Our approach for making this comparison is based upon extended analysis of variations in aerosol and scattering observed at different tower altitudes. We argue that breaking-wave events (Fig. 1) measured at 5 m have similar timescales and surface foam exposure as those on the reef. The impact of the larger ''reef'' breaking waves on lidar extinction downwind of the reef is assumed to be similar in character and duration to the 5-m tower data but decreases during transport away from the reef (Porter et al. 2003). We also assume that the 20-m tower data reflect open-ocean conditions and should correspond to minimum values in lidar extinction when the impact from reef breaking waves is negligible. Hence, lidar extinction data collected between the reef and the coast should have values that fall between extinction determined from our 5- and 20-m tower data. In order to convert lidar measurements into aerosol scattering coefficients we used a constrained forward step-

ping (CFS) approach (Porter et al. 2000, 2003) with accuracy claimed at better than 35%.

During each 2-min vertical lidar scan, the data were averaged (5 s) over a swath 25 m high and 100 m along the beam located about 300–400 m out from the tower at an angle of 58° (toward the reef; Fig. 1b). At a nominal wind speed of 10 m s^{-1} about 100 linear meters of air will pass our sample inlet for each 10-s sample interval in the tower data. This means a single measurement representing the lidar ''swath'' is generally comparable to two 5-s in situ data points measured at the tower. Even so, values between the surface and 25 m are mixed in the lidar swath and parcels of this air may or may not move inland toward the tower. As mentioned previously, during SEAS the airflow from the most active reef area tended to pass north of the tower. Aerosol plumes from the reef area could also lift quickly, mix, and dilute during passage to the tower (Porter et al. 2003). However, minimum values in lidar and tower extinction data should reflect values least influenced by recent breaking waves. At the same time, pronounced increases in lidar values caused by aerosol plumes from the reef regions should approach peak excursions in tower extinction data associated with the coastal waves as characterized at the 5-m tower height. Horizontal lidar data along the beach (Porter et al. 2003) show that aerosol from waves reaches to only about 4 m high near the water's edge, but with perturbed flow over the research vans at the tower (Fig. 1a) these plumes were clearly evident in our 5-m data (Figs. 2, 3) but perhaps diluted compared to undisturbed plumes. Nevertheless, the range of values measured at 5 m is expected to bound lidar values at 300 m and reveal similar overall trends.

Given the good agreement established between measured nephelometer extinction and the values calculated from the size distributions, both the continuous nephelometer and size-derived extinction, after correcting both to ambient conditions, should bracket the range of variations in lidar extinction. However, in order to compare nephelometer extinction to lidar extinction it must be corrected for aerosol growth to ambient humidity. This growth results in increased scattering that varies with composition and size distribution. The dependence of the ratio of wet to dry scattering with RH is expressed as f(RH), as shown in Fig. 9. This includes examples of sea salt, sea salt and sulfate, and mixtures of sea salt and pollution (Massling et al. 2003). The sea-salt and sulfate mix was used to adjust scattering to ambient conditions, and the fit to the SEAS curve above 45% RH is given by $f(\mathrm{RH}) = 1.45(1 - \mathrm{RH}) - 0.48$ for $45\% < \mathrm{RH} < 95\%$.

Figure 10 includes UH nephelometer data corrected to obtain the expected ambient scattering extinction after allowing for angular truncation (Anderson and Ogren 1998), sampling losses, and f(RH) for the SEAS period, as discussed earlier. Because the nephelometer did not measure some of the largest aerosols because of the inlet losses discussed previously, the measured scattering will

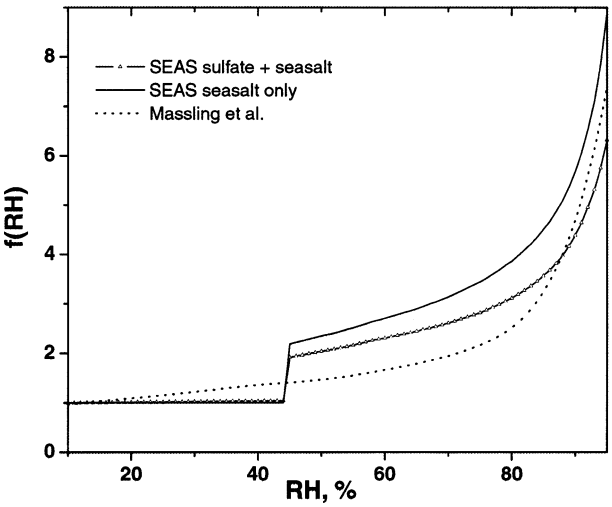

FIG. 9. Humidity-dependent scattering, f(RH).

be less than it should be. However, on the basis of size-dependent losses characterized above, we estimate that about a 55% average expected increase in measured scattering values is needed to represent ambient conditions. This has been applied to the ambient nephelometer values shown. Continuous scattering data for 5-m data reveal the high values and large variability associated with intermittent breaking waves, in contrast to the much lower and less variable data for the 20-m sampling. Also shown are extinction values calculated from the size distributions taken from 5 and 20 m and corrected to ambient conditions. Values for the ambient 20-m calculated extinction (Fig. 10, red squares) are consistent with the ambient corrected nephelometer values. The size-derived extinction at 5 m (20-min average) for breaking waves (triangles) also often shows good agreement and is generally bounded by excursions in the 5-m nephelometer data.

Lidar extinction (5-s average taken every 2 min) for the 25 m by 100 m lidar swath are shown (when available) in Fig. 10 as open circles while values for a similar swath located at 1600 m near the reef are shown as green squares. The lower envelope of many lidar values falls near the 20-m extinction values obtained from the size distributions and nephelometer extinction data (e.g., DOYs 114.6–115, 115.5–116.5, 119.3–119.6, 121.4–121.6). However, lidar values at 300-m distance frequently show excursions to somewhat higher values in these periods that are not seen in the 20-m tower data. The larger excursions in lidar data measured at 1600 m near the reef generally fall within the highly variable 1–2-min nephelometer extinction peaks at 5 m (also see Fig. 2) and close to the averaged (20 min) size-distribution extinction measured at 5 m (triangles). Sequential elevated lidar values often range quickly over several minutes, consistent with plume features meandering in and out of the lidar box (see Fig. 2) that is being sampled every 2 min. Hence, both minimum and maximum val-

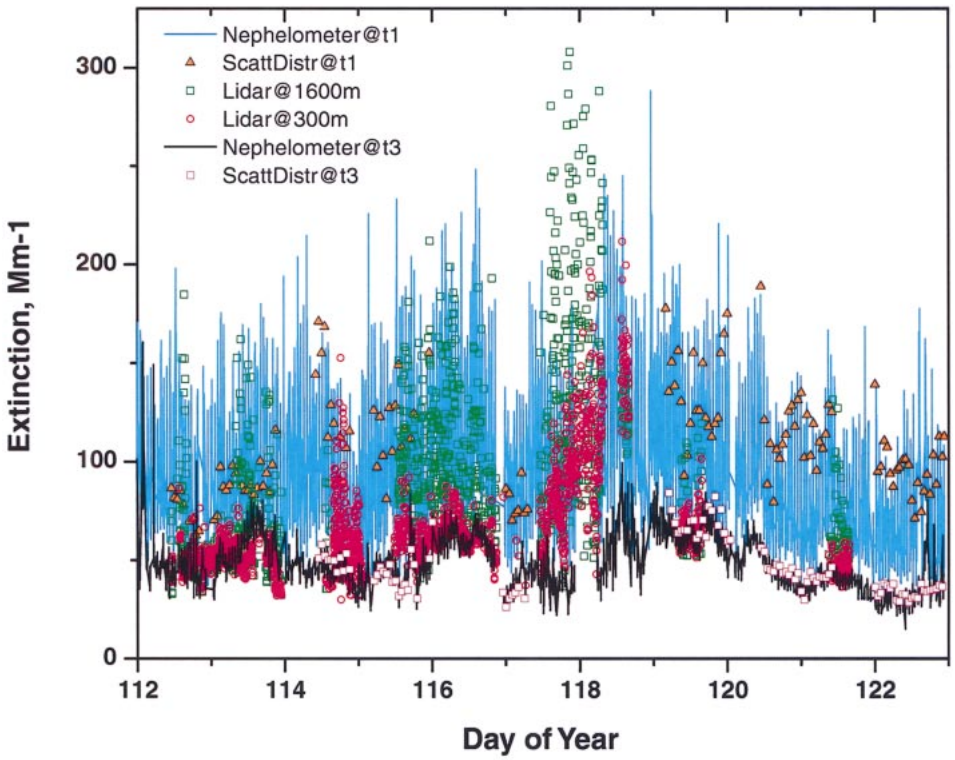

FIG. 10. Time series of 5-m (t1) continuous extinction data (blue lines) and 20-m (t3) extinction data (black lines) corrected to ambient conditions. Corresponding extinction calculated with 20-min averages from size distribution at t1 (triangles) and t3 (red open boxes) compared to variations in lidar extinction observed 300 m offshore from 0–25 m (circles) and at 1600 m offshore near the reef (green open boxes).

ues measured by the lidar are consistent with measurements made on the tower for open-ocean and near-breaking-wave conditions.

b. Statistical characteristics of extinction data

This range of lidar extinction is also evident in the bimodal lognormal frequency distribution of near-surface extinction values. These are shown (Fig. 11) for 20–26 April during SEAS at a range of 1600 m (0–25 m) immediately downwind of the reef (Porter et al. 2003) and at 300 m away from the tower. At 1600 m the most frequent lidar extinction values are seen near 50 and 100 Mm^{-1}. The latter is dominated by extinction from recent breaking waves and can be expected to be broad and variable since it represents an average over the lidar swath. Also, because it can include near-surface contributions below 5 m, it is not surprising that the peak extinction value can at times be higher than the 5-m tower data (t1). Because the elevated extinction values contributed by reef aerosol depend on both the size and the concentration of the aerosol, we expect that sedimentation of the larger sizes and dilution through mixing will decrease peak extinction values downwind. At 300 m this larger mode remains evident but is reduced in frequency compared to values near 50 Mm^{-1}. This is consistent with the observation that during many periods the minimum lidar values are similar to 20-m extinction values (Fig. 10).

An extinction mode from breaking waves is also evident in the lowest 5-m tower (t1) data and with a peak frequency similar to the lidar near 100 Mm^{-1}. Though maximum scattering is less than the maximum lidar val-

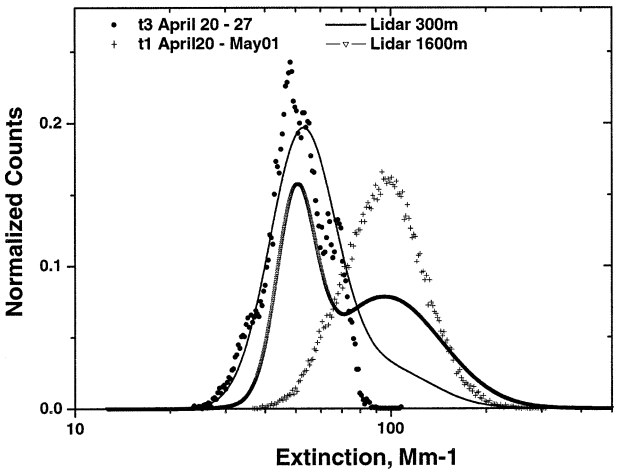

FIG. 11. Frequency plots for extinction values inferred by lidar near the reef at 1600 m (triangle) and 300 m (line) and extinction from size distributions at tower base (t1) for breaking waves and at tower top (t3).

ues at 1600 m, it is clearly lognormal and close to the most frequent value. Calculated extinction (0.55 μm) for the size distributions (dots) from 20 m (t3) is shown for the same time periods as the lidar data, and most frequent extinction values in the 40–50 Mm^{-1} range agree with the most frequent minimum values seen in lidar data at both 300 and 1600 m. In spite of this remarkable agreement we should be aware of the following.

1) In situ values calculated from sizes may be in error due to underrepresented coarse particles, uncertain model assumptions, and/or sizing errors estimated at ±20% by Clarke et al. (2002).
2) Lidar calibration errors are estimated at ±25% (Porter et al. 2003).
3) Values determined at 20 m on the tower are not equivalent to concurrent lidar data measured at 300 m, since the latter is integrated over 0–25 m at 58° azimuth and closer to the path of typical plumes passing north of the tower (e.g., Fig. 2 of Clarke and Kapustin 2003).

In spite of these uncertainties, these data demonstrate closure between extinction values estimated from the nephelometer, modeled from size distributions, and inferred from lidar to within expected errors.

5. Conclusions

By sampling sequentially at three tower altitudes over an extended period we were able to characterize the size distributions derived from individual near-surface, breaking-wave events from the background marine aerosol. Isolating these events by means of a LAG chamber and applying thermal analysis to identify their refractory properties, we were able to demonstrate that particles from breaking waves were produced in all sizes from 10 nm to greater than 10 μm. These distributions were similar for heated and unheated distributions, confirming the particles' refractory nature at 360°C and consistent with them being sea salt.

The typical number concentrations for integrated size distributions measured about 20 m downwind of small breaking-wave events were in the range of 30–50 cm^{-3} and consistent with spikes in concurrently collected total CN number concentrations. The shape of this number distribution is also similar to the refractory distribution characteristic of the open-ocean data collected at the top of the tower (Fig. 4). This suggests that small sea-salt particles from open-ocean breaking waves may contribute significantly to open-ocean particle number and become incorporated into mixed refractory and volatile particles through heterogeneous chemical reaction on the sea-salt surface and/or coagulation with a more volatile aerosol often entrained from above the marine boundary layer (Clarke et al. 1996). Due to the high diffusivity of the smaller sea salt particles produced by breaking waves, it is likely that many will be removed to a preexisting marine aerosol surface while the larger aerosol could readily act as cloud condensation nuclei under typical marine conditions.

Small coastal breaking waves also produced particles larger than 1 μm, as are commonly observed. These contributions were at far lower concentrations (on the order of 1 cm^{-3}) but interact effectively with visible light and generally enhance the aerosol light scattering (0.55 μm) by about a factor of 2 at 5 m and about 20 m downwind of the water's edge. The production of larger sea-salt aerosol can dominate scattering extinction in a coastal setting over moderate spatial scales when breaking waves are present. In pursuing this topic we also demonstrated that performance characteristics of the TSI3020 APS resulted in artifact sizing at larger sizes compared to the newer TSI3021 model.

Offshore variability in response to breaking waves was also evident in lidar data obtained near the reef. Long-term comparisons were made between the range of extinction values obtained by lidar between the reef and tower and the range of extinction values at the tower for both nearshore breaking waves measured at 5 m and unperturbed values made at 20 m. These were consistent with observed nephelometer extinction values and those derived from the measured size distributions to within combined measurement uncertainty. In most cases the lidar extinction values ranged between measured in situ tower data for background and breaking-wave extinction. This confirms that lidar extinction values are consistent with tower-derived ambient extinction values to within the 25% uncertainty identified in this lidar calibration technique.

Acknowledgments. We extend special appreciation to Drs. R. Ferek and S. Ackleson of the Office of Naval Research for their support (N00014-96-1-0320) of our long-term measurements at BAFS and of the SEAS experiment described here.

REFERENCES

Anderson, T. L., and J. A. Ogren, 1998: Determining aerosol radiative properties using the TSI 3563 integrating nephelometer. *Aerosol Sci. Technol.,* **29,** 57–69.

Berner, A., C. H. Lurzer, F. Pohl, O. Preining, and P. Wagner, 1979: The size distributions of urban aerosols in Vienna. *Sci. Total Environ.,* **13,** 245–261.

Campuzano-Jost, P., and Coauthors, 2003: Near-real-time measurement of sea-salt aerosol during the SEAS campaign: Comparison of emission-based sodium detection with an aerosol volatility technique. *J. Atmos. Oceanic Technol.,* **20,** 1421–1431.

Clarke, A. D., 1991: A thermo-optic technique for in-situ analysis of size-resolved aerosol physicochemistry. *Atmos. Environ.,* **25A,** 635–644.

——, and J. N. Porter, 1993: Pacific marine aerosol. Part II: Equatorial gradients, ammonium and chlorophyll during SAGA3. *J. Geophys. Res.,* **98,** 16 997–17 010.

——, and V. N. Kapustin, 2003: The Shoreline Environment Aerosol Study (SEAS): A context for marine aerosol measurements influenced by a coastal environment and long-range transport. *J. Atmos. Oceanic Technol.,* **20,** 1351–1361.

——, Z. Li, and M. Litchy, 1996: Aerosol dynamics in the Pacific marine boundary layer: Microphysics, diurnal cycles, and entrainment. *Geophys. Res. Lett.*, **23,** 733–736.

——, J. L. Varner, F. Eisele, R. Tanner, L. Mauldin, and M. Litchy, 1998: Particle production in the remote marine atmosphere: Cloud outflow and subsidence during ACE-1. *J. Geophys. Res.*, **103,** 16 397–16 409.

——, and Coauthors, 2002: The INDOEX aerosol: A comparison and summary of microphysical, chemical, and optical properties observed from land, ship, and aircraft. *J. Geophys. Res.*, **107,** 8033, doi:10.1029/2001JD000572.

de Leeuw, G., F. Neele, M. Hill, M. Smith, and E. Vignati, 2000: Production of sea-spray aerosol in the surf zone. *J. Geophys. Res.*, **105,** 29 397–29 409.

Hand, J. L., R. B. Ames, S. M. Kreidenweis, D. E. Day, and W. C. Malm, 2000: Estimates of particle hygroscopicity during the Southeastern Aerosol and Visibility Study. *J. Air Waste Manage. Assoc.*, **50,** 677–685.

Hoppel, W. A., G. M. Frick, and J. W. Fitzgerald, 2002: Surface source function for sea-salt aerosol and aerosol dry deposition to the ocean surface. *J. Geophys. Res.*, **107,** 4832, doi:10.1029/2001JD002014.

Masonis, S., T. Anderson, D. Covert, V. Kapustin, A. Clarke, S. Howell, and K. Moore, 2003: A study of the extinction-to-backscatter ratio of marine aerosol during the Shoreline Environment Aerosol Study. *J. Atmos. Oceanic Technol.*, **20,** 1388–1402.

Massling, A., A. Wiedensohler, B. Busch, C. Neusüss, P. Quinn, T. Bates, and D. Covert, 2003: Hygroscopic properties of different aerosol types over the Atlantic and Indian Oceans. *Atmos. Chem. Phys. Discuss.*, **3,** 135–185.

Porter, J. N., B. Lienert, and S. K. Sharma, 2000: Using the horizontal and slant lidar calibration methods to obtain aerosol scattering coefficients from a coastal lidar in Hawaii. *J. Atmos. Oceanic Technol.*, **17,** 1445–1454.

——, ——, ——, and E. Lau, 2003: Vertical and horizontal aerosol scattering fields over Bellows Beach, Oahu, during the SEAS experiment. *J. Atmos. Oceanic Technol.*, **20,** 1375–1387.

Quinn, P. K., D. J. Coffman, T. S. Bates, T. L. Miller, J. E. Johnson, K. Voss, E. J. Welton, and C. Neusüss, 2001: Dominant aerosol chemical components and their contribution to extinction during the Aerosols99 cruise across the Atlantic. *J. Geophys. Res.*, **106,** 20 783–20 810.

Reid, J. S., H. Jonsson, M. Smith, and A. Smirnov, 2001: Evolution of the vertical profile and flux of large sea-salt particles in a coastal zone. *J. Geophys. Res.*, **106,** 12 039–12 053.

Stelson, A. W., 1990: Urban aerosol refractive index prediction by partial molar refraction approach. *Environ. Sci. Technol.*, **24,** 1676–1679.

Swietlicki, E., and Coauthors, 2000: Hygroscopic properties of aerosol particles in the north-eastern Atlantic during ACE-2. *Tellus*, **52B,** 201–227.

Tang, I. N., A. C. Tridico, and K. H. Fung, 1997: Thermodynamic and optical properties of sea salt aerosol. *J. Geophys. Res.*, **102,** 23 269–23 275.

Vignati, E., G. de Leeuw, and R. Berkowicz, 2001: Modeling coastal aerosol transport and effects of surf-produced aerosols on processes in the marine boundary layer. *J. Geophys. Res.*, **106,** 20 225–20 238.

Zhang, S. H., Y. Akutsu, L. M. Russell, R. C. Flagan, and J. H. Seinfeld, 1995: Radial differential mobility analyzer. *Aerosol Sci. Technol.*, **23,** 357–371.